

# Stokes shift/emission efficiency trade-off in donor-acceptor perylenemonoimides for luminescent solar concentrators†

Cite this: DOI: 10.1039/c5ta01134e

Riccardo Turrisi,<sup>a,c</sup> Alessandro Sanguineti,<sup>a</sup> Mauro Sassi,<sup>a</sup> Brett Savoie,<sup>c</sup> Atsuro Takai,<sup>c</sup> Giorgio E. Patriarca,<sup>a</sup> Matteo M. Salamone,<sup>a</sup> Riccardo Ruffo,<sup>a</sup> Gianfranco Vaccaro,<sup>a</sup> Francesco Meinardi,<sup>a</sup> Tobin J. Marks,<sup>c</sup> Antonio Facchetti<sup>b</sup> and Luca Beverina<sup>\*a</sup>

Perylenediimides (PDIs) are among the best performing organic luminescent materials, both in terms of emission efficiency and chemical and photochemical stability because of their rigid, symmetric and planar structure; however, they exhibit very small Stokes shifts. The sizeable reabsorption of the emitted light limits the performances of perylenediimides in imaging applications and luminescent solar concentrators. Perylenemonoimides (PMIs) having an electron donating substituent in one of the free *peri* positions feature larger Stokes shift values while retaining high chemical stability. The selection of the most appropriate donor, both in terms of electron donating capability and steric demand, boosts emission efficiency and limits reabsorption losses. The synthesis, optical spectroscopy, molecular orbital computations, UPS, electrochemical, spectroelectrochemical, and multinuclear NMR investigation of a series of PMI derivatives functionalized with donors having different electronic characteristics and steric demands are discussed. Results are relevant for the fabrication of single layer plastic luminescent solar concentrators (LSC).

Received 11th February 2015  
Accepted 20th February 2015

DOI: 10.1039/c5ta01134e

[www.rsc.org/MaterialsA](http://www.rsc.org/MaterialsA)

## Introduction

Perylene dyes are among the most successful  $\pi$ -conjugated organic derivatives for optoelectronic applications. Their most relevant features include flexibility in chemical structures, tuning of electrical, optical and optoelectronic properties, low toxicity, high absorption and emission efficiencies as well as unrivalled photo, thermal and chemical stabilities.<sup>1–5</sup> As such, perylene dyes have found applications in diverse research fields such as organic field effect transistors,<sup>6–10</sup> dye lasers,<sup>11</sup> donor-acceptor dyads,<sup>12,13</sup> sensors,<sup>14,15</sup> imaging and bioimaging,<sup>16–18</sup> nonlinear optics<sup>19–21</sup> and dye sensitized<sup>22–25</sup> and bulk heterojunction solar cells.<sup>26,27</sup> Perylenediimides (PDIs), under the brand name of Lumogen, are also the core active component of luminescent solar concentrators (LSCs), a class of light concentrating devices introduced in the early 70s and recently

revisited in view of their applicability in building integrated photovoltaics.<sup>28–31</sup>

The LSC concept was introduced to reduce production costs and overcome some limitations of standard silicon-based photovoltaics without changing the basic photon-to-current conversion technology (silicon single junction cells). Moreover, these devices possess building integration opportunities, which are even greater than those of large area dye sensitized solar cells. In their most common embodiment, LSCs are slabs of transparent, high-quality optical materials doped with luminescent molecules.<sup>32</sup> The host material is typically poly(methylmethacrylate) (PMMA), although in specific cases other materials can be used.<sup>33,34</sup> The embedded luminescent molecules absorb sunlight and emit light inside the slab. If the refractive index of the slab is significantly higher than that of the air, most of the emitted light will be trapped by total internal reflection. The emitted light will travel to the slab edges, and it will be collected there in a small area, where a standard silicon solar cell is located. The advantages of such a strategy are as follows: (1) the LSC is a light collector, where diffused light over a large area is concentrated at the slab edges; this is useful because silicon PV cells need a certain light intensity threshold to convert light into electricity. (2) The amount of silicon in the cell can be reduced because silicon is required only to cover the LSC slab edges. (3) The slabs can be easily integrated with buildings due to their wide colour tuning capabilities. If properly engineered, a LSC can be a structural component (for

<sup>a</sup>Department of Materials Science, Università di Milano-Bicocca, via Cozzi 55, 20125, Milano, Italy. E-mail: [luca.beverina@unimib.it](mailto:luca.beverina@unimib.it)

<sup>b</sup>Polyera Corporation, 8045 Lamon Avenue, Suite 140, Skokie, IL 60077, USA

<sup>c</sup>Department of Chemistry and the Argonne-Northwestern Solar Energy Research Center, Northwestern University, Evanston, Illinois, 60208, USA

† Electronic supplementary information (ESI) available: Synthetic procedures for the preparation of derivatives 1–4. Copy of the <sup>1</sup>H and <sup>13</sup>C NMR for all the new compounds. Details on computational investigation. Details on electrochemical, UPS and time-resolved emission characterizations. Details on PMMA samples preparation. Details on the photodegradation of derivative 1. See DOI: 10.1039/c5ta01134e

example in sunroofs and windows), an active energy-producing device and a decorative element at the same time.

The main limitation of the LSC concept is the re-absorption of the emitted light due to incomplete spectral separation between dye absorption and emission spectra.<sup>35</sup> This effect strongly limits the maximum collecting efficiency of the slab's surface. Recently, Curie *et al.* demonstrated that the use of bilayer structures consisting of a thin film of organic dyes vacuum deposited on a high-refractive-index glass efficiently reduces re-absorption losses.<sup>36</sup> Further optimizations of the LSC structure have also been recently proposed.<sup>31,37–39</sup> Low-cost, plastic, single layer LSCs require the design of efficient luminophores, having complete spectral separation between absorption and emission (*i.e.* large Stokes shifts). Moreover, the dye should absorb the largest possible portion of the solar spectrum and efficiently emit in the slab as well as withstand direct exposure to solar light and possibly extreme weather conditions for years. Among various chromophore classes for LSCs (namely, rhodamines<sup>28</sup> and coumarins,<sup>40</sup> oligothio-phenes,<sup>33</sup> phycobilisomes,<sup>41</sup> lanthanide chelates<sup>42–47</sup> and, more recently, quantum dots<sup>38,48–50</sup>) perylenediimides represent the **state-of-the-art** class in LSC materials, even though their Stokes Shift is very small.<sup>51,52</sup>

Molecules featuring a large Stokes shift pertain to two main classes, having in common a large change in the molecular structure upon optical excitation (Fig. S1, ESI†): (a) donor–acceptor derivatives (D–A) and (b) twisted (TW) structures. In D–A derivatives, the optical transition involves a redistribution of the electron density from an electron-rich group (the donor) to an electron-poor one (the acceptor) through a conjugated bridge.<sup>53–56</sup> To date, this is the broadest class of derivatives with large Stokes shifts that find various applications, for example in fluorescence bio-imaging.<sup>57,58</sup> Efficient D–A fluorophores feature rigid, planar and easily polarizable conjugated bridges, allowing large changes in the electronic distribution upon optical excitation.

Conversely, TW molecules possess conjugated bridges having substantial deviations from planarity. The *p*-terphenyl molecule represents a good example of this class of materials (see Fig. S1†). Optical excitation involves a transition from the aromatic and twisted ground state structure to a quinoidal excited state structure having formal double bonds connecting the neighboring benzene rings. The resulting major variations in the molecular electronic structure translate into a large Stokes shift.<sup>59,60</sup> The PDI core cannot be manipulated to fit in either of two such classes, while perylenemonoimides (PMIs) can display a rather pronounced D–A character, provided that they carry a strong electron donating substituent in one or both free *peri* positions.<sup>53,61–66</sup> Moreover, substitution at the same positions with bulky arenes leads to TW-type structures having relevant Stokes shifts, as demonstrated by the PMI dimers prepared by the Langhal's group.<sup>67</sup>

In specific cases, *i.e.* when the arene introduced at one of the free *peri* positions is bulky and is also a donor group, the resulting PMI will behave according to a combination of the D–A and TW governed regimes. The capability to control the interplay of the TW *vs.* D–A contributions in PMIs could provide

a tool for the further optimization of these compounds for LSC applications. In fact, twisted structures usually feature high fluorescence efficiency and modest molar absorptivity, while donor–acceptor compounds exhibit opposite behaviour.

The present paper aims at studying the influence of the electronic and steric characteristics of donor residue on the Stokes shift and emission efficiency in a series of PMIs (1–5, Fig. 1) for a single layer LSC. These derivatives were investigated by steady-state UV-vis absorption and emission spectroscopies, UV-vis transient absorption spectroscopy, electrochemistry, spectroelectrochemistry, UPS and multinuclear NMR measurements to establish general structure–property relationships. We also investigated how the molecular properties dominate single layer LSC efficiencies with particular emphasis on reabsorption losses.

## Chromophore design and synthesis

Fig. 1 shows the chemical structure of the PMI derivatives investigated in this study along with those of the planar/rigid derivative **PMI-qs**<sup>68</sup> used here for comparison. Derivatives 1–5 share the same PMI core and differ in the donor group at the *peri* position. Aimed at establishing structure–property relationships that govern the emission efficiency and extent of the Stokes shift, we selected a series of donor groups sharing, except for derivative **1**, the same donating centre, a nitrogen atom featuring an available lone pair, embedded in very diverse electronic structures.

In detail, molecule **1** features an indolizine donor, where the nitrogen lone pair involved in the substituent  $\pi$  orbital makes the pentatomic ring  $\pi$ -excessive, and thus electron donating. The molecule is connected to the PMI core through its 1-position. This is the only member of this series featuring a carbon–carbon bond between the donor and the perylene core. Molecule **2** possesses a carbazole donor directly connected to the perylene core through the nitrogen atom. Because the central ring of carbazole is aromatic, the nitrogen lone pair that is involved in the carbazole  $\pi$  orbital is not particularly prone to delocalization towards the PMI electron-withdrawing end. Derivatives **3** and **4** have already been described in the literature as D–A molecules.<sup>53,64,65</sup> In terms of donating capabilities, it can

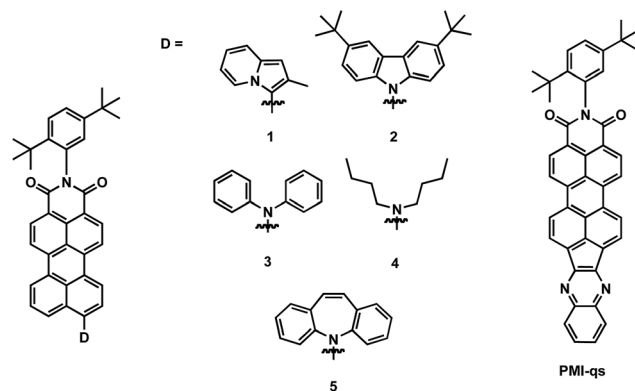


Fig. 1

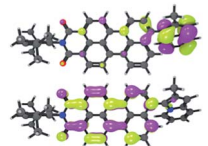
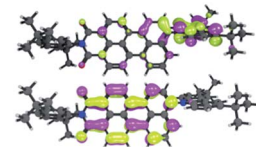
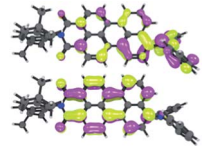
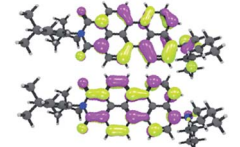
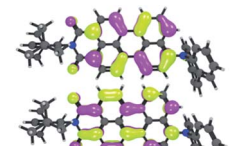
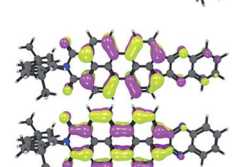
be anticipated that a dialkylamine will be a stronger donor due to the lack of delocalization of the nitrogen lone pair over aryl substituents rather than the perylene core.<sup>69</sup> Moreover, derivative **4** is the only member of the series that can be described as a purely D–A molecule without TW contribution. Finally, derivative **5** features a dibenzoazepine donor, which is directly connected with the perylene core through its nitrogen atom. The central ring of dibenzoazepine features 8  $\pi$ -electrons, and therefore as per Hückel's definition, it is antiaromatic. Thus, the nitrogen lone pair should be extremely prone to delocalization because the donation of the electron pair would provide aromatic stabilization. It should be noted that the Hückel rule applies for monocyclic, planar compounds. The case of dibenzoazepine is different, and thus deviations from purely antiaromatic behaviour are expected.<sup>70</sup>

The synthesis of derivatives **1–5** is reported in Scheme S1 of the ESI.† The key intermediate for all of the compounds is the unsubstituted perylene monoimide **7**. The latter can be prepared, according to the method proposed by Langhals, *i.e.*, by the condensation/decarboxylation reaction between **perylendianhydride 6** and 3,5-di-*tert*-butylaniline.<sup>71</sup> This reaction was carried out in the presence of Zn(AcO)<sub>2</sub> using imidazole as the solvent in a steel autoclave at 190 °C for 24 h. Pure **6** can be isolated in 33% yield after chromatographic purification. The regioselective bromination of **6**, according to the Nagao procedure, gives the bromide **8** in 91% yield after chromatographic purification.<sup>72</sup> Derivative **1** was prepared by the direct arylation of 2-methylindolizine with bromide **8**. These types of reactions are preferred because they do not require toxic chemicals, and the removal of organometallic intermediates is easy, generally giving high yields, once the reaction conditions are optimized.<sup>73</sup> We obtained the best results working under Fagnou conditions,<sup>74</sup> *i.e.*, using DMAc at 100 °C with Pd(AcO)<sub>2</sub>/P(cyclohexyl)<sub>3</sub>HBF<sub>4</sub> as the catalyst in the presence of pivalic acid and K<sub>2</sub>CO<sub>3</sub> as a base. Unlike all other compounds in the series, derivative **1** proved to be unstable in air. The Buchwald–Hartwig amination of **8** with 4,7-di-*tert*-butylcarbazole, diphenylamine, dibutylamine and dibenzoazepine gives derivatives **2** (41%), **3** (70%), **4** (70%) and **5** (75%), respectively. The reaction conditions were the same for all of the compounds: we used a Pd(dba)<sub>2</sub>/P(*t*Bu)<sub>3</sub> catalyst in refluxing toluene with *tert*-BuONa as the base. We carried out these reactions for 6–8 h under microwave irradiation. The conversion was complete in all of the cases, whereas the reaction yields reflected the nucleophilicity of the donor nitranion.

## Molecular orbital computations

To obtain insights into the electronic structure and geometry of the PMI derivatives, particularly molecular planarity upon donor variation, we carried out molecular orbital computations.<sup>75</sup> All the DFT calculations were performed using the Q-Chem software suite; details are discussed in the ESI.†<sup>76</sup> Table 1 shows the calculated ground state geometries, HOMO and LUMO energies, torsional angle between the donor and perylene core and the dipole moments of derivatives **1–5** and of reference molecule **PMI-qs**. Derivatives **1** and **2** that feature the

Table 1 Optimized HOMO and LUMO geometries (B3LYP/6-31G\*\*), energies, torsional angle formed between perylene core and donor residue and ground state dipole moment for derivatives **1–5** and **PMI-qs**

PMI	HOMO (up) LUMO (down)	Torsional angle (°)	$\mu$ (Debye)
<b>1</b>		61	5.93
<b>2</b>		62	4.75
<b>3</b>		45	6.70
<b>4</b>		—	8.14
<b>5</b>		80	5.98
<b>PMI-qs</b>		0	3.51

planar and rigid indolizine and carbazole donating groups, respectively, exhibit remarkably large torsional angles with respect to the perylene core (61° and 62°, respectively). MO calculations give a ground state dipole moment, which is higher for derivative **1** (5.93 Debye) than for derivative **2** (4.75 Debye). Derivative **3**, having a diphenylamine donating group, is also considerably twisted (45°) and shows a calculated dipole moment of 6.70 Debye, which is higher than that of both **1** and **2**. Finally, the structure of derivative **5** shows that initially the central ring of the dibenzoazepine residue is considerably bent (its two benzene rings forming an angle of 122°); this data is consistent with the reported X-ray structure.<sup>70</sup> Moreover, the whole dibenzoazepine residue is almost perpendicular with respect to the perylene plane (80° of torsional angle). The dipole moment for derivative **5** is calculated to be 5.98 Debye, lower than that of **3**, as expected due to the severe deviation from

planarity. With the exclusion of derivative **4** (dipole moment 8.14 Debye), a purely D–A compound, all the other molecules can be described as the combinations of donor–acceptor and twisted structures. In fact, all of them show a sizeable deviation from planarity (like in the case of *p*-terphenyl discussed in the Introduction and shown in Fig. S1†).

At the same time, the variation in the ground state molecular dipole moment as a function of the type of donor group (increasing in the order  $2 < 1 < 5 < 3 < 4$ ) indicates the presence of D–A behaviour (similar to that of DCM, Fig. S1†).

## Electrochemical, spectroelectrochemical, UPS and transient absorption characterizations

Inspection of the differential pulse voltammetry (DPV) plots of a D–A compound family that possesses the same acceptor and conjugated core enabled us to rank the donating capabilities of a donor series. In this study, we used DPV instead of the more commonly employed cyclic voltammetry (CV) because some of our PMIs do not exhibit reversible oxidations (Fig. 2a and b show the DPV plots, Fig. S2 of the ESI† shows the corresponding CV plots for all the compounds). Donating substituents are expected to increase the electrochemically-derived HOMO energies according to their specific donating strengths. Furthermore, if the donor and the acceptor ends are efficiently coupled, an increasing donating strength should also increase the LUMO energy because the accepting end, where most likely the LUMO is localized, becomes harder to reduce. Thus, when a particular donor mostly affects the HOMO energy without

altering the LUMO, its coupling with the acceptor (and the extent of the  $\pi$ -conjugation) may be considered weak. The likely reasons for such behaviour are excessive bridge conjugation length and/or the presence of a sizeable torsional angle between the donor and the acceptor (the acceptor being, at least in our case, forced to be coplanar with the bridge). As such, the simultaneous inspection of both reduction and oxidation processes in a molecule series enables the donor strength to be ranked in terms of electron density effectively transferred towards the acceptor. It is worth noting that DPV is not a direct vertical ionization technique; consequently, the solvent stabilization of charged species, as well as the reorganization energy, always have an impact on the electrochemically-derived HOMO and LUMO levels.<sup>69</sup> Thus, in parallel with electrochemical techniques, we also employed ultraviolet photoemission spectroscopy (UPS)—a vertical ionization technique—and compared the results (Fig. 2c and d). All DPV, UPS, and the resulting molecular orbital energies are collected in Table 2 along with corresponding calculated values.

DPV plots (Fig. 2a and b) show that derivative **1**, the only compound exhibiting poor air stability, features the lowest oxidation potential in this series (+0.25 V vs.  $\text{Fc}^+/\text{Fc}$ ), compared with those of **2** (+0.79 V), **3** (+0.52 V), and **4** (+0.29 V), which are located at higher potentials. Thus, the electrochemically-derived HOMO energy of derivative **1** (−5.48 eV) is higher than those of derivatives **2–4** (**2**: −6.02 eV; **3**: −5.75 eV; and **4**: −5.52 eV). Amongst the nitrogen-based donors, the dibutylamine is the strongest one (derivative **4**) followed by the diphenylamine (derivative **3**) and next by the carbazole. Interestingly, the use of dibenzoazepine (derivative **5**), a supposedly very strong donor, leads to an electrochemical HOMO (−5.59 eV) intermediate between those of **3** and **4**. This result can be rationalized by the peculiar geometry of compound **5** (see previous paragraph). **Dibutylamine remains the stronger nitrogen-based donor because its nitrogen lone pair can be fully delocalized over the perylene bridge because they are not shared by any other conjugated residue.** The electrochemical LUMO levels (Table 2) show the same trend as the corresponding HOMOs, even though the differences in the corresponding energies are less pronounced, as expected by the calculated LUMOs, whose major contributions come from the perylene core.

We compared DPV results with solvent-independent UPS data. We included in the experiment the strongly electron-deficient derivative **PMI-qs**, which was previously used for luminescent solar concentrators. Fig. 2c shows the high-binding energy cut-off region of the normalized photoemission spectra at −9 V bias for compounds **1**, **2**, **3**, **5** and **PMI-qs**. The full photoemission spectra are reported in Fig. S9 of the ESI.† The ionization potential of all the solids is equal to the difference between the high-binding (low kinetic) cut-off energies and the low-binding (high-kinetic) Fermi edge onsets. Fig. 2d shows the low-binding energy cut-off region that highlights the difference in the first ionization shoulder (*vide infra*).

Table 2 shows the comparison between UPS ionization potentials and the corresponding calculated and electrochemical HOMO levels. The trend for derivatives **1**, **2** and **3** is

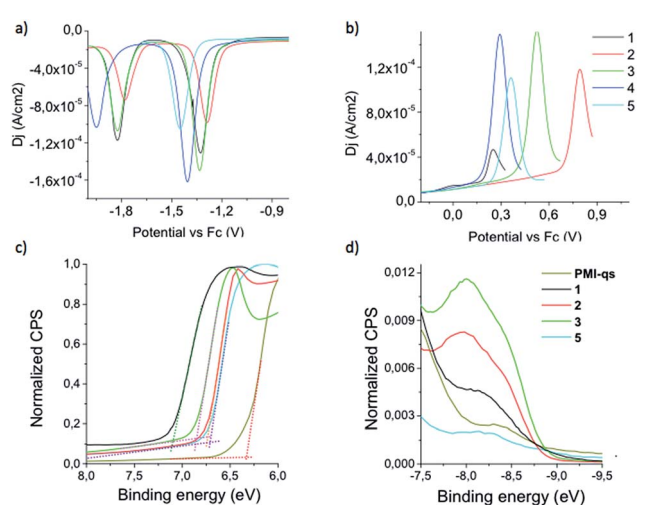


Fig. 2 Electrochemical and UPS characterization of derivatives **1–5**. Reduction (a) and oxidation (b) DPV plots for derivatives **1–5** in  $\text{CH}_2\text{Cl}_2$  with tetrabutylammonium *p*-toluenesulfonate as the supporting electrolyte. (c) Normalized photoemission spectra under a −9 V bias for compounds **1**, **2**, **3**, **5** and the reference derivative **PMI-qs** in the high-binding energy cut-off region. The onset for all the spectra has been moved to −8.92 eV to evidence the arising difference in ionization potentials. (d) Low-binding energy cut-off region highlighting the difference in the first ionization shoulder.



Table 2 Comparison between the calculated, electrochemical and UPS estimations of the HOMO and LUMO levels for derivatives 1–5 and PMI-qs

	1	2	3	4	5	PMI-qs
$E_{pc}^{red}$ (V vs. $Fc^+/Fc$ )	-1.32	-1.29	-1.33	-1.41	-1.45	-1.84
$E_{pc}^{ox}$ (V vs. $Fc^+/Fc$ )	0.25	0.79	0.52	0.29	0.36	—
Electrochemical HOMO (eV)	-5.48	-6.02	-5.75	-5.52	-5.59	—
Electrochemical LUMO (eV)	-3.65	-3.62	-3.66	-3.74	-3.78	-4.17
UPS HOMO (eV)	-5.20	-5.60	-5.45	—	-5.60	-5.95
Calculated HOMO	-5.09	-5.36	-5.17	-5.20	-5.47	-5.71
Calculated LUMO	-2.80	-2.88	-2.75	-2.64	-2.80	-3.18

consistent with the DPV data. The deviations between the datasets are possibly ascribed to solvent/aggregation effects associated with the DPV experiments. However, in our case, the UPS and DPV datasets are almost superimposable for derivative 5. Moreover, UPS- and oxidation potential-derived HOMO energies for 5 and 2 are the same. In addition, on examining the low-binding energy region of the UPS spectra (Fig. 2d), we can notice that 1, 2 and 3 show a shoulder attributed to the first ionization process, while both PMI-qs and 5 show a weaker signal. The absence of a peak is expected for PDI-qs—an all acceptor compound—this result is unexpected for 5. As observed previously for the naphthalene analogue of 5, the molecule is so severely twisted that D–A charge transfer becomes strongly impaired.<sup>77</sup> In the solid state, derivatives 2 and 5 share the same deep HOMO level (–5.60 eV), closer to that of the all-acceptor derivative PMI-qs (–5.95 eV).

Conversely, the DPV data place the HOMO energy of derivative 5 well above that of derivatives 2 and 3. This inconsistency questions the real charge transfer nature of the HOMO–LUMO transition of derivative 5. Indeed, the inspection of the orbital densities of 5 in the gas phase suggests a marginal role for the donor group in both the ground and the first excited state electron densities (Table 1). Such conflicting data can be explained by taking into account a likely different geometry of 5 in solution with respect to both the solid state and the gas phases. However, to better characterize the nature of the HOMO–LUMO transition of 5 in solution, we carried out time-resolved transient absorption experiments in deaerated dichloromethane at room temperature and we compared the results with spectroelectrochemical analysis in the same solvent.

The transient spectra of 5 in the 500–700 nm region show intense absorption bands at 566 and 638 nm (Fig. 3). Bleaches (negative  $\Delta A$ ) at  $\lambda < 520$  nm and  $\lambda > 700$  nm are due to ground state depletion and stimulated emission, respectively. The decay time of the absorption bands at 566 and 638 nm is in the order of a few nanoseconds. The absorption band at 638 nm decays with a first-order rate constant of  $3.7 \times 10^{10} \text{ s}^{-1}$  (Fig. 4a), while the change in the absorption at 566 nm occurs in two steps with first-order rate constants of  $3.7 \times 10^{10} \text{ s}^{-1}$  and  $2.3 \times 10^8 \text{ s}^{-1}$  (see Fig. S11 and S12 of the ESI†). The initial fast process may be attributed to a conformational change of (5)\* (e.g. increased planarity and  $sp^3 \rightarrow$  pseudo- $sp^2$  geometry of the linking dibenzoazepine nitrogen).<sup>78</sup>

please replace with a arrow

A direct excitation of the dibenzoazepine moiety and the consequent energy transfer from PMI-1dibenzoazepine\* to 1PMI\*-dibenzoazepine should be excluded because the dibenzoazepine moiety does not absorb in the 480 nm region (*i.e.* the excitation wavelength). Subsequently, the signal decays according to a charge-transfer process from the dibenzoazepine donor to the PMI acceptor, in agreement with the D–A behaviour. These spectra correspond to the sum of the reduced (radical anion) and oxidized (radical cation) forms of 5 as obtained by a spectroelectrochemical experiment (Fig. 4). The rate constant of the charge transfer process ( $2.3 \times 10^8 \text{ s}^{-1}$ ; 4.3 ns) is consistent with the fluorescence lifetime of analogous PMI derivatives ( $\sim 3$  ns).<sup>79</sup>

## Multinuclear NMR investigation

Multinuclear  $^1\text{H}$  and  $^{13}\text{C}$  NMR spectroscopies can be of further aid in characterizing the effective electron donating capabilities of our donors. In fact, the inspection of the chemical shift of selected positions across the perylene bridge provides qualitative information about the amount of charge that a given donor is conveying towards the acceptor.

This effect is distinct from and complementary to the HOMO energy increase evidenced by electrochemical and UPS techniques. NMR will monitor an increase in the charge transfer

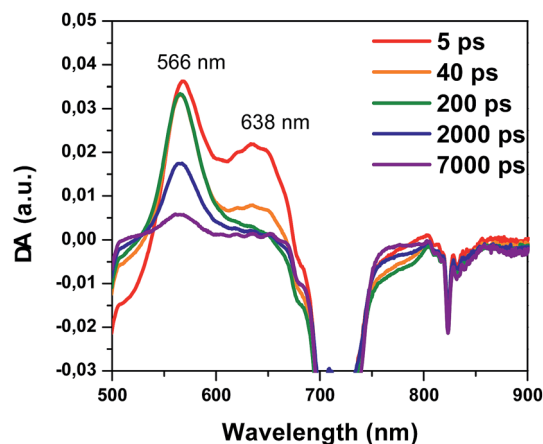


Fig. 3 Differential transient absorption spectra of 5 ( $1.5 \times 10^{-5} \text{ M}$ ) for 7 to 7000 ps after laser pulse irradiation at 480 nm in deaerated dichloromethane at 298 K.

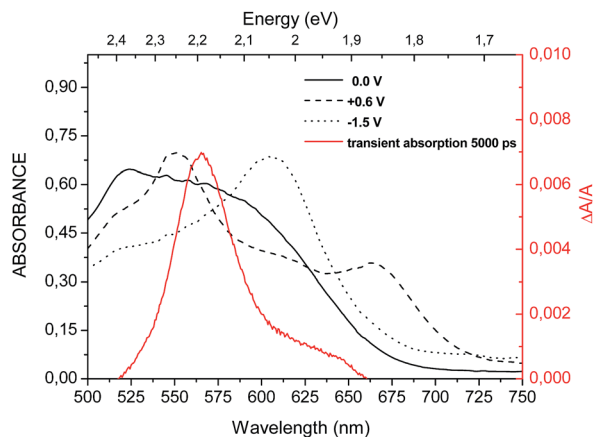


Fig. 4 Comparison between the transient absorption spectrum at 5000 ps of a dichloromethane solution of **5** and the corresponding spectroelectrochemical absorption spectra of a  $\text{CH}_3\text{CN}$  solution of the same compound at no applied bias (solid line),  $-1.5$  V (dotted line) and  $+0.6$  V (dashed line). Potentials are reported versus the  $\text{Fc}/\text{Fc}^+$  redox couple.

character through the chemical shift variations of the perylene core. We considered particularly meaningful positions, namely **6** and **6b**, which are highlighted in the quinoidal forms (**2**) and (**3**) of the top part of Fig. 5. In fact, according to the relative contribution of the aromatic versus quinoidal canonical description of the PMI ground state, the selected positions will show an upfield shift proportional to the donating strength of the employed donor.<sup>69,80,81</sup>

Table S1 of the ESI† summarizes the  $^1\text{H}$  and  $^{13}\text{C}$  NMR data for the positions **5**, **6**, **7**, **8** and **6b** of the perylene core for **1–5**. Detailed inspection of all the data shows the same trend, more or less pronounced, for all the positions: an upfield shift of the  $^1\text{H}$  and  $^{13}\text{C}$  NMR signals in the order  $2 < 1 < 3 < 4 < 5$ . We will discuss in particular the data referring to the  $^{13}\text{C}$  signals of positions **6b**. This particular carbon is quaternary and

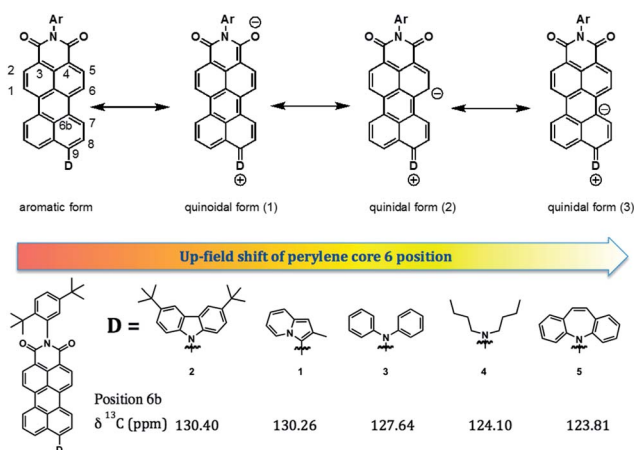


Fig. 5 Top: canonical representations of a general PMI highlighting the delocalization of donor charge on positions **6** and **6b**. Bottom: ranking of the donating capabilities of different donors according to the  $^{13}\text{C}$  chemical shift of carbon **6b**.

unaffected by through-space effects. Moreover, as it is shown in the quinoidal form (**3**) of Fig. 5, in one of the canonical representations of the general structure of our PMIs, the charge residing on the donor can be delocalized in that position. Thus, the  $^{13}\text{C}$  signal of position **6b** for derivative **2** (130.40 ppm) is essentially the same as that of the corresponding signal for derivative **1** (130.26 ppm). This result reflects the inefficiency of indolizine to act as a  $\pi$  donor, even though such residue is strongly electron rich (and thus easily oxidized) in electrochemical terms. The signal for derivative **3** (127.64 ppm) is considerably upfield shifted, according to the documented donating capabilities of aromatic amines. The signal for derivative **4** is even more upfield shifted (124.10 ppm). Exactly as in the case of the electrochemical ranking of donating capability, the NMR data confirm that an alkyl amine is a stronger donor than an aryl one.<sup>69</sup> Finally, the signal for derivative **5** experiences the highest upfield shift in the series (123.81 ppm), confirming that the dibenzoazepine residue is a stronger donor, at least in solution, as compared to a standard aromatic amine, and its donating capability is comparable to aliphatic amines. The inspection of both  $^1\text{H}$  and  $^{13}\text{C}$  signals of positions **6** and **8** shows the same trend with the only exception being position **8** of derivative **4**, which is considerably upfield shifted with respect to the other compounds in the series. The deviation can be associated with the fact that this derivative is the only one featuring an alkyl substituent and is thus unaffected by through-space shielding effects that are instead affecting the position **8** of all the other compounds.

## UV-vis absorption and emission spectroscopy

Fig. 5 shows the absorption (left) and emission (right) spectra of **1–5** in  $\text{CHCl}_3$  and Table 3 summarizes all the UV-vis characterization data. Literature data shows that D–A PMIs are characterized by a broad and featureless absorption band peaking at 500–650 nm, sizeable Stokes shifts (3000–4000  $\text{cm}^{-1}$ ) and generally low emission efficiencies (<40%).<sup>53,64</sup>

This holds true for derivatives **3** and **4**, with **4** outperforming **3** in terms of Stokes shift by 750  $\text{cm}^{-1}$ . The absorption spectrum of **5** is also broad but with a distinguishable vibronic structure. The latter feature is related to less pronounced charge transfer behavior with respect to both **3** and **4**, as corroborated by the smaller Stokes shift (2560  $\text{cm}^{-1}$ ). In contrast to all the other PMIs, derivative **2** possesses a vibrationally structured absorption and a broad and featureless emission. Moreover, its Stokes shift (3790  $\text{cm}^{-1}$ ) is nearly as large as that of **4** (3814  $\text{cm}^{-1}$ ), even though carbazole hardly qualifies as a strong donor. Likewise, **2** is the only derivative in the series, which behaves mostly as a TW derivative with very little D–A character. Upon optical excitation, this molecule undergoes a quinoidal distortion, enforcing molecular planarity. The resulting major difference between the ground and first excited electronic states is responsible for the particularly large Stokes shift.

Derivatives **1** and **2** exhibit similar torsional angles; the notable difference is that indolizine in **1** is a stronger donor.

This has profound consequences in terms of optical properties and photostability. The close inspection of the absorption spectrum of derivative **1** shows that its band is made of two contributions, a high energy absorbing, vibrationally structured one peaking at 504 nm and a low energy absorbing shoulder around 570 nm. The Stokes shift is unusually small ( $1436\text{ cm}^{-1}$ ).

Moreover, the vibrationally resolved component of both the absorption and the emission bands of **1** closely resembles that of the unsubstituted (donor = H) PMI **7** (see structure in Scheme S1†). Interestingly, Fig. S8 of the ESI† shows that upon exposure to direct sunlight in an air-equilibrated solution, the spectrum of **1** becomes superimposable on that of **7**. We believe that the low energy component of the absorption of derivative **1** corresponds to a through-space photoinduced charge transfer from the indolizine residue to the PMI core with consequent formation of an air-unstable indolizine radical cation and a PMI radical anion. The anion can be reversibly quenched by molecular oxygen, while the radical cation undergoes irreversible degradation.<sup>82</sup> Such a mechanism can be possibly applied for all electron-rich and strongly twisted substituents. Fig. S13† shows a cartoon highlighting the tentative mechanism for the observed degradation.

Analysis of the emission efficiencies is also particularly meaningful. First of all, derivative **4** is the only compound whose (low) emission efficiency does not change appreciably on going from toluene to chloroform solutions. This is essentially a D–A chromophore, and thus it exhibits low emission efficiency (39% and 33% in toluene and  $\text{CHCl}_3$ , respectively) and a large Stokes shift. For all the other compounds, the emission efficiency is significantly higher in toluene (99%, 95% and 73% for

**Table 3** UV-vis molar extinction coefficients, absorption and emission maxima, luminescence quantum yields and Stokes shifts for derivatives 1–5 in toluene and  $\text{CHCl}_3$  solutions. Luminescence quantum yields in PMMA slabs. Derivative **1** was not embedded in PMMA slabs for stability reasons

Compound	$\lambda_{\text{max}}$ abs (nm)	$\lambda_{\text{max}}$ fluo (nm)	$\phi_i$	$\epsilon$ ( $\text{L mol}^{-1}\text{ cm}^{-1}$ )	Stokes shift ( $\text{cm}^{-1}$ )
<b>1</b> ( $\text{CHCl}_3$ )	502	541	<5%	25 600	1436
<b>2</b> (toluene)	513	578	99%	32 000	2192
<b>2</b> ( $\text{CHCl}_3$ )	517	643	43%	33 000	3790
<b>2</b> (PMMA) <sup>a</sup>			93%		
<b>3</b> (toluene)	550	629	95%	31 500	2284
<b>3</b> ( $\text{CHCl}_3$ )	560	676	56%	31 000	3064
<b>3</b> (PMMA) <sup>a</sup>			73%		
<b>4</b> (toluene)	530	654	39%	28 000	3577
<b>4</b> ( $\text{CHCl}_3$ )	550	696	33%	29 000	3814
<b>4</b> (PMMA) <sup>a</sup>			40%		
<b>5</b> (toluene)	562	646	73%	30 000	2314
<b>5</b> ( $\text{CHCl}_3$ )	577	677	36%	29 000	2560
<b>5</b> (PMMA) <sup>a</sup>			70%		

<sup>a</sup> Absorption maxima of the slabs are not reported because the LSC demonstrators were too absorptive for UV-vis spectrometers. Emission maxima depend on the distance with respect to the excitation point (see next section).

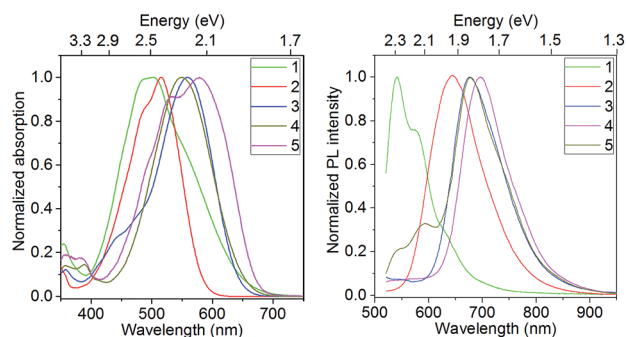


**Fig. 6** Normalized absorption (left) and emission (right) spectra of derivatives 1–5 in  $\text{CHCl}_3$ .

derivatives **2**, **3** and **5**, respectively) than in chloroform (43%, 56% and 36% for **2**, **3** and **5**, respectively).

Indeed, solvent polarity influences the interplay between D–A and TW regimes because a polar solvent (chloroform) will enhance the former contribution, while a low polarity one (toluene) will do the opposite. Coherently, for all the compounds possessing sizeable torsional angles (see Table 1) between the donor and the acceptor, low polarity solvents lead to higher luminescence quantum yields. For the purpose of the proposed application, the data in PMMA are particularly meaningful. In this case, the emission efficiency will depend not only on polarity, as in the case of solutions, but also on viscosity. In fact, molecules possessing two conjugated fragments connected by a single bond having restricted rotational freedom frequently behave as “molecular rotors”. The most distinctive characteristic of such a class of compounds is an increase in the luminescence quantum yield upon increasing the local viscosity.<sup>60</sup> In particular, we recently introduced a naphthalene analogue of derivative **5** as a very efficient molecular rotor that is capable of probing the nanostructure of core-shell nanoparticles obtained through the self-assembly of amphiphilic block copolymers (Fig. 6).<sup>77</sup>

Indeed, with the sole exception of derivative **4** (a further confirmation of the purely donor–acceptor nature of this compound), all emission quantum yields in PMMA are systematically higher than the values in chloroform, and in general, they are comparable with those in toluene, even though the polarity of PMMA is even higher than that of chloroform. The value is particularly high for derivative **2**; this is again not surprising because this is almost a purely twisted compound, and thus a molecular rotor. As derivative **2** combines a very high Stokes shift and the highest quantum yield in the series, we tested its performance as the luminophore in a LSC prototype.

## Luminescent solar concentrator devices

A  $10^{-4}\text{ M}$  solution in PMMA/MMA syrup of derivative **2** was heated in a cell cast immersed in a water bath at  $56\text{ }^\circ\text{C}$  for 48 h. The cell cast was then annealed at  $100\text{ }^\circ\text{C}$  for 12 h (see ESI†). During the whole process, the sample remained homogeneous

without showing any sign of precipitation/phase segregation. The slab was characterized in terms of solid state quantum yield and re-absorption losses as a function of the distance between the excitation point and the slab edge, where emitted light was collected. It is worthwhile to note that derivative 2 in a PMMA matrix is almost as efficient (93%) as the reference Lumogen f 240 orange dye (perylene-3,4,9,11-tetracarboxylic acid bis-(2',6'-diisopropylanilide), quantum yield 99%).<sup>68</sup>

Several processes, including light scattering at the interfaces or inside the slab itself and photoluminescence re-absorption, affect the LSC efficiency. To isolate the optical losses due to the re-absorption, which are strictly related to the active dye efficiency, we plotted the evolution of the normalized emission spectrum as a function of the distance between the detection at the LSC edge and the excitation spot (laser operating @ 405 nm). The normalization was carried out on the low-energy tail of the spectrum ( $\lambda > 730$  nm), where the re-absorption is negligible (Fig. 7a). The PL spectrum shifts towards lower energies when the distance is increased; however, the overall intensity is only slightly attenuated, as clearly shown in Fig. 7b. Thus, for an optical path of 10 cm, the LSC based on derivative 2 retains about 80% of its initial intensity. Fig. 7b also reports the scattering losses obtained from the attenuation of a laser at 820 nm (photon energy below the band gap) traveling through the slab (Fig. 7c). The scattering contribution is generally very small and constant throughout the sample; this is additional evidence

that any further improvement of LSC performances will mostly depend on the optimization of the luminophore properties in terms of Stokes shift and luminescence quantum yield.

## Conclusions

Our findings demonstrate that derivative 2 represents an optimal trade-off because it shows both a very large Stokes shift and a high emission quantum yield. This compound represents a significant entry in the field of luminescent materials for LSC, and it is a valid alternative to the traditional Lumogen dyes for the fabrication of larger area devices. Indeed, Fig. 7d compares the estimated total PL output as a function of the LSC size for the slabs doped with derivative 2 and with Lumogen f 240 orange. As expected, the tendency of the total emitted light to saturate by increasing the device dimensions is rather small for both LSC devices, whose performances are indistinguishable within the experimental uncertainties, even though the luminescence quantum yield for derivative 2 is considerably smaller. The use of the latter in any case is advantageous as its red-shifted emission spectrum corresponds to the region of maximum external quantum yield of silicon solar cells.

## Acknowledgements

Authors gratefully acknowledge the financial support of "Fondazione Cariplo" through grant 2010-0564 "Luminescent Solar Concentrators for Building Integrated Photovoltaics-LumiPhoto".

## Notes and references

- 1 C. Huang, S. Barlow and S. R. Marder, *J. Org. Chem.*, 2011, **76**, 2386–2407.
- 2 F. Würthner and M. Stolte, *Chem. Commun.*, 2011, **47**, 5109–5115.
- 3 X. Zhan, A. Facchetti, S. Barlow, T. J. Marks, M. A. Ratner, M. R. Wasielewski and S. R. Marder, *Adv. Mater.*, 2011, **23**, 268–284.
- 4 C. Liu, C. Xiao, Y. Li, W. Hu, Z. Li and Z. Wang, *Chem. Commun.*, 2014, **50**, 12462–12464.
- 5 T. Weil, T. Vosch, J. Hofkens, K. Peneva and K. Müllen, *Angew. Chem., Int. Ed.*, 2010, **49**, 9068–9093.
- 6 L. Ferlauto, F. Liscio, E. Orgiu, N. Masciocchi, A. Guagliardi, F. Biscarini, P. Samori and S. Milita, *Adv. Funct. Mater.*, 2014, **24**, 5503–5510.
- 7 K. Trofymchuk, A. Reisch, I. Shulov, Y. Mély and A. S. Klymchenko, *Nanoscale*, 2014, **6**, 12934–12942.
- 8 R. C. Savage, E. Orgiu, J. M. Mativetsky, W. Pisula, T. Schnitzler, C. L. Eversloh, C. Li, K. Müllen and P. Samori, *Nanoscale*, 2012, **4**, 2387.
- 9 G. Griffini, L. Brambilla, M. Levi, M. Del Zoppo and S. Turri, *Sol. Energy Mater. Sol. Cells*, 2013, **111**, 41–48.
- 10 J. E. Anthony, A. Facchetti, M. Heeney, S. R. Marder and X. Zhan, *Adv. Mater.*, 2010, **22**, 3876–3892.

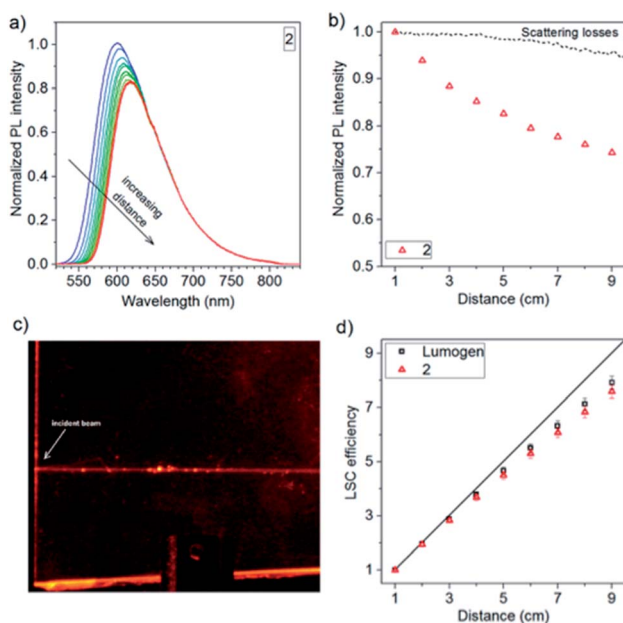


Fig. 7 (a) PL spectra excited at 405 nm as a function of distance (from 1 to 10 cm) between the excitation spot and detection at LSC edge for derivative 2; (b) integrated PL output signal as a function of the distance from the excitation spot for derivatives 2. For comparison, the scattering losses, obtained from the diffusion of a laser beam at 820 nm travelling through a pure PMMA slab (c), are also reported. (d) Total PL output for a linear growth of the slab size for an LSC based on derivative 2, and for reference, an LSC based on Lumogen f 240 is also investigated. The black-line indicates the "hypothetic" PL output increase for an ideal lossless sample.



- 11 L. Cerdán, A. Costela, G. Durán-Sampedro, I. García-Moreno, M. Calle, M. Juan-y-Seva, J. de Abajo and G. A. Turnbull, *J. Mater. Chem.*, 2012, **22**, 8938–8947.
- 12 P.-O. Schwartz, L. Biniek, E. Zaborova, B. Heinrich, M. Brinkmann, N. Leclerc and S. Méry, *J. Am. Chem. Soc.*, 2014, **136**, 5981–5992.
- 13 J. M. Mativetsky, M. Kastler, R. C. Savage, D. Gentilini, M. Palma, W. Pisula, K. Müllen and P. Samori, *Adv. Funct. Mater.*, 2009, **19**, 2486–2494.
- 14 Z. Liu, C. Tonnelé, G. Battagliarin, C. Li, R. A. Gropeanu, T. Weil, M. Surin, D. Beljonne, R. Lazzaroni, M. Debliquy, J.-M. Renoirt and K. Müllen, *J. Phys. Chem. B*, 2014, **118**, 309–314.
- 15 D. Görl, X. Zhang and F. Würthner, *Angew. Chem., Int. Ed.*, 2012, **51**, 6328–6348.
- 16 A. Sarbu, L. Biniek, J.-M. Guenet, P. J. Mésini and M. Brinkmann, *J. Mater. Chem. C*, 2015, **3**, 1235–1242.
- 17 T. Ribeiro, S. Raja, A. S. Rodrigues, F. Fernandes, C. Baleizão and J. P. S. Farinha, *Dyes Pigm.*, 2014, **110**, 227–234.
- 18 S. Fery-Forgues, *Nanoscale*, 2013, **5**, 8428.
- 19 M. M. Sartin, C. Huang, A. S. Marshall, N. Makarov, S. Barlow, S. R. Marder and J. W. Perry, *J. Phys. Chem. A*, 2014, **118**, 110–121.
- 20 Z. An, S. A. Odom, R. F. Kelley, C. Huang, X. Zhang, S. Barlow, L. A. Padilha, J. Fu, S. Webster, D. J. Hagan, E. W. Van Stryland, M. R. Wasielewski and S. R. Marder, *J. Phys. Chem. A*, 2009, **113**, 5585–5593.
- 21 X. Huang, Q. Shi, W.-Q. Chen, C. Zhu, W. Zhou, Z. Zhao, X.-M. Duan and X. Zhan, *Macromolecules*, 2010, **43**, 9620–9626.
- 22 J. Fortage, M. Séverac, C. Houarner-Rassin, Y. Pellegrin, E. Blart and F. Odobel, *J. Photochem. Photobiol., A*, 2008, **197**, 156–169.
- 23 C. Li, A. Keerthi, Z. Liu, Y. Liu, J. Schöneboom, Q. Wang, F. Eickemeyer, S. Valiyaveetil, N. G. Pschirer, P. Erk, A. Herrmann and K. Müllen, *J. Mater. Chem.*, 2009, **19**, 5405–5415.
- 24 T. Edvinsson, T. Edvinsson, C. Li, C. Li, N. Pschirer, N. Pschirer, J. Schoneboom, J. Schoneboom, F. Eickemeyer, F. Eickemeyer, R. Sens, R. Sens, G. Boschloo, G. Boschloo, A. Herrmann, A. Herrmann, K. Mullen, K. Mullen, A. Hagfeldt and A. Hagfeldt, *J. Phys. Chem. C*, 2007, **111**, 15137–15140.
- 25 L. Le Pleux, A. L. Smeigh, E. Gibson, Y. Pellegrin, E. Blart, G. Boschloo, A. Hagfeldt, L. Hammarström and F. Odobel, *Energy Environ. Sci.*, 2011, **4**, 2075.
- 26 E. Kozma and M. Catellani, *Dyes Pigm.*, 2013, **98**, 160–179.
- 27 C. Li and H. Wonneberger, *Adv. Mater.*, 2012, **24**, 613–636.
- 28 M. G. Debije and P. P. C. Verbunt, *Adv. Energy Mater.*, 2012, **2**, 12–35.
- 29 W. G. J. H. M. van Sark, K. W. J. Barnham, L. H. Slooff, A. J. Chatten, A. Büchtemann, A. Meyer, S. J. McCormack, R. Koole, D. J. Farrell, R. Bose, E. E. Bende, A. R. Burgers, T. Budel, J. Quillit, M. Kennedy, T. Meyer, C. D. M. Donegá, A. Meijerink and D. Vanmaekelbergh, *Opt. Express*, 2008, **16**, 21773–21792.
- 30 B. Rowan, L. Wilson and B. Richards, *IEEE J. Quantum Electron.*, 2008, **14**, 1312–1322.
- 31 H. Hernandez-Noyola, D. Potterveld, R. Holt and S. B. Darling, *Energy Environ. Sci.*, 2012, **5**, 5798–5802.
- 32 L. Beverina and A. Sanguineti, *Sol. Cell Nanotechnol.*, 2013, **317**–356.
- 33 V. Fattori, M. Melucci, L. Ferrante, M. Zambianchi, I. Manet, W. Oberhauser, G. Giambastiani, M. Frediani, G. Giachi and N. Camaioni, *Energy Environ. Sci.*, 2011, **4**, 2849–2853.
- 34 M. Melucci, M. Durso, L. Favaretto, M. L. Capobianco, V. Benfenati, A. Sagnella, G. Ruani, M. Muccini, R. Zamboni, V. Fattori and N. Camaioni, *RSC Adv.*, 2012, **2**, 8610–8613.
- 35 J. C. Goldschmidt, M. Peters, A. Bösch, H. Helmers, F. Dimroth, S. W. Glunz and G. Willeke, *Sol. Energy Mater. Sol. Cells*, 2009, **93**, 176–182.
- 36 M. J. Currie, J. K. Mapel, T. D. Heidel, S. Goffri and M. A. Baldo, *Science*, 2008, **321**, 226–228.
- 37 N. D. Boscher, P. Choquet, D. Duday, N. Kerbellec, J.-C. Lambrechts and R. Maurau, *J. Mater. Chem.*, 2011, **21**, 18959–18961.
- 38 R. H. Inman, G. V. Shcherbatyuk, D. Medvedko, A. Gopinathan and S. Ghosh, *Opt. Express*, 2011, **19**, 24308–24313.
- 39 V. M. Agranovich, Y. N. Gartstein and M. Litinskaya, *Chem. Rev.*, 2011, **111**, 5179–5214.
- 40 L. Slooff, E. Bende, A. Burgers, T. Budel, M. Pravettoni, R. Kenny, E. Dunlop and A. Büchtemann, *Phys. Status Solidi RRL*, 2008, **2**, 257–259.
- 41 C. L. Mulder, L. Theogarajan, M. Currie, J. K. Mapel, M. A. Baldo, M. Vaughn, P. Willard, B. D. Bruce, M. W. Moss, C. E. McLain and J. Morseman, *Adv. Mater.*, 2009, **21**, 3181–3185.
- 42 S. F. H. Correia, V. de Zea Bermudez, S. J. L. Ribeiro, P. S. André, R. A. S. Ferreira and L. D. Carlos, *J. Mater. Chem. A*, 2014, **2**, 5580–5596.
- 43 A. Sanguineti, A. Monguzzi, G. Vaccaro, F. Meinardi, E. Ronchi, M. Moret, U. Cosentino, G. Moro, R. Simonutti, M. Mauri, R. Tubino and L. Beverina, *Phys. Chem. Chem. Phys.*, 2012, **14**, 6445–6448.
- 44 J. Graffion, A. M. Cojocariu, X. Cattoën, R. A. S. Ferreira, V. R. Fernandes, P. S. André, L. D. Carlos, M. W. C. Man and J. R. Bartlett, *J. Mater. Chem.*, 2012, **22**, 13279–13285.
- 45 C. Freund, W. Porzio, U. Giovanella, F. Vignali, M. Pasini, S. Destri, A. Mech, S. Di Pietro, L. Di Bari and P. Mineo, *Inorg. Chem.*, 2011, **50**, 5417–5429.
- 46 X. Wang, T. Wang, X. Tian, L. Wang, W. Wu, Y. Luo and Q. Zhang, *Sol. Energy*, 2011, **85**, 2179–2184.
- 47 O. Moudam, B. C. Rowan, M. Alamiry, P. Richardson, B. S. Richards, A. C. Jones and N. Robertson, *Chem. Commun.*, 2009, 6649.
- 48 C. S. Erickson, L. R. Bradshaw, S. McDowall, J. D. Gilbertson, D. R. Gamelin and D. L. Patrick, *ACS Nano*, 2014, **8**, 3461–3467.
- 49 F. Meinardi, A. Colombo, K. A. Velizhanin, R. Simonutti, M. Lorenzon, L. Beverina, R. Viswanatha, V. I. Klimov and S. Brovelli, *Nat. Photonics*, 2014, **8**, 392–399.

- 1 50 F. Purcell-Milton and Y. K. Gun'ko, *J. Mater. Chem.*, 2012, **22**, 16687–16697.
- 51 W. E. Benjamin, D. R. Veit, M. J. Perkins, E. Bain, K. Scharnhorst, S. McDowall, D. L. Patrick and J. D. Gilbertson, *Chem. Mater.*, 2014, **26**, 1291–1293.
- 52 C. Haines, M. Chen and K. P. Ghiggino, *Sol. Energy Mater. Sol. Cells*, 2012, **105**, 287–292.
- 53 P. D. Zoon and A. M. Brouwer, *Photochem. Photobiol. Sci.*, 2009, **8**, 345–353.
- 10 54 G. Brusatin, P. Innocenzi, A. Abbotto, L. Beverina, G. A. Pagani, M. Casalboni, F. Sarcinelli and R. Pizzoferrato, *J. Eur. Ceram. Soc.*, 2004, **24**, 1853–1856.
- 55 P. V. Bernhardt, R. Koch, D. W. J. Moloney, M. Shtaiwi and C. Wentrup, *J. Chem. Soc., Perkin Trans. 2*, 2002, 515–523.
- 15 56 S. R. Marder, L. T. Cheng, B. G. Tiemann, A. C. Friedli, M. Blanchard-Desce, J. W. Perry and J. Skindhoj, *Science*, 1994, **263**, 511–514.
- 57 X. Feng, P. Wu, F. Bolze, H. Leung, K. Li, N. Mak, D. Kwong, J. Nicoud, K. Cheah and M. Wong, *Org. Lett.*, 2010, **12**, 2194–2197.
- 20 58 P. Salice, S. Versari, S. Bradamante, F. Meinardi, G. Macchi, G. A. Pagani and L. Beverina, *Organic Photonics and Photovoltaics*, 2013, **2013**, 39–55.
- 25 59 I. López-Duarte, T. T. Vu, M. A. Izquierdo, J. A. Bull and M. K. Kuimova, *Chem. Commun.*, 2014, **50**, 5282–5284.
- 60 N. Amdursky, Y. Erez and D. Huppert, *Acc. Chem. Res.*, 2012, **45**, 1548–1557.
- 61 E. J. Alexy, J. M. Yuen, V. Chandrasher, J. R. Diers, C. Kirmaier, D. F. Bocian, D. Holten and J. S. Lindsey, *Chem. Commun.*, 2014, **50**, 14512–14515.
- 30 62 Y. Zagranjarski, L. Chen, Y. Zhao, H. Wonneberger, C. Li and K. Müllen, *Org. Lett.*, 2012, **14**, 5444–5447.
- 63 C. Jiao, K.-W. Huang, C. Chi and J. Wu, *J. Org. Chem.*, 2011, **76**, 661–664.
- 35 64 C. Li, J. Schöneboom, Z. Liu, N. G. Pschirer, P. Erk, A. Herrmann and K. Müllen, *Chem.–Eur. J.*, 2009, **15**, 878–884.
- 65 P. D. Zoon and A. M. Brouwer, *ChemPhysChem*, 2005, **6**, 1574–1580.
- 40 66 N. Tasios, C. Grigoriadis, M. R. Hansen, H. Wonneberger, C. Li, H. W. Spiess, K. Müllen and G. Floudas, *J. Am. Chem. Soc.*, 2010, **132**, 7478–7487.
- 45 67 H. Langhals and A. Hofer, *J. Org. Chem.*, 2012, **77**, 9585–9592.
- 68 A. Sanguineti, M. Sassi, R. Turrise, R. Ruffo, G. Vaccaro, F. Meinardi and L. Beverina, *Chem. Commun.*, 2013, **49**, 1618–1620.
- 69 O. Kwon, S. Barlow, S. A. Odom, L. Beverina, N. J. Thompson, E. Zojer, J.-L. Brédas and S. R. Marder, *J. Phys. Chem. A*, 2005, **109**, 9346–9352.
- 70 M. T. Reetz, S. Htte, R. Goddard and U. Minet, *J. Chem. Soc., Chem. Commun.*, 1995, 275–277.
- 5 71 H. Langhals, G. Schonmann and L. Feiler, *Tetrahedron Lett.*, 1995, **36**, 6423–6424.
- 72 Y. Nagao, Y. Abe and T. Misono, *Dyes Pigm.*, 1991, **16**, 19–25.
- 73 A. Facchetti, L. Vaccaro and A. Marrocchi, *Angew. Chem., Int. Ed.*, 2012, **51**, 3520–3523.
- 10 74 B. Ligault, D. Lapointe, L. Caron, A. Vlassova and K. Fagnou, *J. Org. Chem.*, 2009, **74**, 1826–1834.
- 75 S. B. Darling, *J. Phys. Chem. B*, 2008, **112**, 8891–8895.
- 76 Y. Shao, L. F. Molnar, Y. Jung, J. Kussmann, C. Ochsenfeld, S. T. Brown, A. T. B. Gilbert, L. V. Slipchenko, S. V. Levchenko, D. P. O'Neill, R. A. DiStasio, R. C. Lochan, T. Wang, G. J. O. Beran, N. A. Besley, J. M. Herbert, C. Y. Lin, T. Van Voorhis, S. H. Chien, A. Sodt, R. P. Steele, V. A. Rassolov, P. E. Maslen, P. P. Korambath, R. D. Adamson, B. Austin, J. Baker, E. F. C. Byrd, H. Dachsel, R. J. Doerksen, A. Dreuw, B. D. Dunietz, A. D. Dutoi, T. R. Furlani, S. R. Gwaltney, A. Heyden, S. Hirata, C.-P. Hsu, G. Kedziora, R. Z. Khalliulin, P. Klunzinger, A. M. Lee, M. S. Lee, W. Liang, I. Lotan, N. Nair, B. Peters, E. I. Proynov, P. A. Pieniazek, Y. M. Rhee, J. Ritchie, E. Rosta, C. D. Sherrill, A. C. Simmonett, J. E. Subotnik, H. L. Woodcock, W. Zhang, A. T. Bell, A. K. Chakraborty, D. M. Chipman, F. J. Keil, A. Warshel, W. J. Hehre, H. F. Schaefer, J. Kong, A. I. Krylov, P. M. W. Gill and M. Head-Gordon, *Phys. Chem. Chem. Phys.*, 2006, **8**, 3172–3191.
- 77 G. Vaccaro, A. Bianchi, M. Mauri, S. Bonetti, F. Meinardi, A. Sanguineti, R. Simonutti and L. Beverina, *Chem. Commun.*, 2013, **49**, 8474–8476.
- 35 78 M. Iwamura, S. Takeuchi and T. Tahara, *J. Am. Chem. Soc.*, 2007, **129**, 5248–5256.
- 79 S. E. Miller, Y. Zhao, R. Schaller, V. Mulloni, E. M. Just, R. C. Johnson and M. R. Wasielewski, *Chem. Phys.*, 2002, **275**, 167–183.
- 40 80 L. M. Tolbert and M. E. Ogle, *J. Am. Chem. Soc.*, 1990, **112**, 9519–9527.
- 81 A. Abbotto, S. Bradamante and G. A. Pagani, *J. Org. Chem.*, 2001, **66**, 8883–8892.
- 45 82 H. Ko, S. Kim, W. Choi, B. Moon and H. Lee, *Chem. Commun.*, 2005, 69–71.
- 50
- 55